Systemic delivery of AAV-GCDH ameliorates HLD-induced phenotype in a glutaric aciduria type I mouse model

Anna Mateu-Bosch,[1,6] Eulàlia Segur-Bailach,[1,2,6] Emma Muñoz-Moreno,[1] María José Barallobre,[1,5] Maria Lourdes Arbonés,[1,5] Sabrina Gea-Sorlí,[1,2] Frederic Tort,[1,2,3] Antonia Ribes,[1,2,3] Judit García-Villoria,[1,2,3] and Cristina Fillat[1,2,4]

[1]Institut d'Investigacions Biomèdiques August Pi i Sunyer (IDIBAPS), 08036 Barcelona, Spain; [2]Centro de Investigación Biomédica en Red de Enfermedades Raras (CIBERER), 08036 Barcelona, Spain; [3]Secció d'Errors Congènits del Metabolisme-IBC, Servei de Bioquímica i Genètica Molecular, Hospital Clínic, 08028 Barcelona, Spain; [4]Facultat de Medicina i Ciències de la Salut. Universitat de Barcelona, 08036 Barcelona, Spain; [5]Instituto de Biología Molecular de Barcelona, IBMB-CSIC, Parc Científic de Barcelona, 08028 Barcelona, Spain

Glutaric aciduria type 1 (GA1) is a rare inherited disorder caused by a deficiency of glutaryl-coenzyme A dehydrogenase (GCDH), with accumulation of neurotoxic metabolites, resulting in a complex movement disorder, irreversible brain damage, and premature death in untreated individuals. While early diagnosis and a lysine restricted diet can extend survival, they do not prevent neurological damage in approximately one-third of treated patients, and more effective therapies are required. Here we report the efficacy of adeno-associated virus 9 (AAV9)-mediated systemic delivery of human GCDH at preventing a high lysine diet (HLD)-induced phenotype in $Gcdh^{-/-}$ mice. Neonatal treatment with AAV-GCDH restores GCDH expression and enzyme activity in liver and striatum. This treatment protects the mice from HLD-aggressive phenotype with all mice surviving this exposure; in stark contrast, a lack of treatment on an HLD triggers very high accumulation of glutaric acid, 3-hydroxyglutaric acid, and glutarylcarnitine in tissues, with about 60% death due to brain accumulation of toxic lysine metabolites. AAV-GCDH significantly ameliorates the striatal neuropathology, minimizing neuronal dysfunction, gliosis, and alterations in myelination. Magnetic resonance imaging findings show protection against striatal injury. Altogether, these results provide preclinical evidence to support AAV-GCDH gene therapy for GA1.

INTRODUCTION

Glutaric aciduria type 1 (GA1; MIM: 231670) is an inborn error of metabolism that was first described in 1975.[1] It has an estimated prevalence of 1 in 100,000 in newborns in the general population, and of 1 in 250 in high-risk populations.[2,3] This disease is caused by mutations in the *GCDH* gene, causing a deficiency of the glutaryl-coenzyme A (CoA) dehydrogenase (GCDH; EC: 1.3.99.7), which is responsible for the dehydrogenation and decarboxylation of glutaryl-CoA in the catabolic pathway of lysine, hydroxylysine, and tryptophan. The human *GCDH* gene is located on chromosome 19p13.2, spans 7 kb,

and consists of 11 exons and 10 introns. The inheritance pattern of GA1 is autosomal recessive, and currently more than 200 mutations in the *GCDH* gene have been identified.[3] GCDH deficiency leads to the accumulation of glutaric acid (GA) and 3-hydroxyglutaric acid (3-OHGA), which are neurotoxic, as well as to an increase of glutarylcarnitine (C5DC), which can deplete carnitine from body fluids and tissues.[4] Untreated individuals mostly develop a complex movement disorder between the ages of 3 and 36 months, due to bilateral striatal damage precipitated by catabolic events such as intercurrent febrile illness or prolonged fasting caused by infections or surgical procedures. After an episode of this type, individuals develop dystonia, choreoathetosis (or choreoathetotic movements), and spasticity, with severe neurological damage typical of an acute encephalopathic crisis.[5] The life expectancy of affected individuals is very variable: some individuals with severe neurological damage can reach adulthood, but approximately one-half of affected children die during their first decade of life during an acute episode.[6–8]

Currently, the only available treatment for individuals with GA1 is based on a lysine-restrictive diet and supplementation of L-carnitine. Despite the possibility of early detection due to the inclusion of GA1 in newborn screening programs and quick treatment initiation, it has still not been possible to prevent cerebral damage totally or disease progression in approximately one-third of individuals with GA1.[2,9,10]

A genetic mouse model of GA1 has been developed to better understand the disease pathology. Mice with complete loss of *GCDH* ($Gcdh^{-/-}$) (herein, knock-out [KO]) are viable, have a normal

A

B

C

appearance, and present a biochemical profile very similar to individuals with GA1: they have high levels of GA and 3-OHGA in urine and brain tissues, and high levels of C5DC in serum.[11] Exposure of *Gcdh* KO mice to elevated levels of dietary protein containing lysine aggravates disease presentation, with tissue and serum accumulation of metabolites and noticeable signs of striatal neurodegeneration. The KO mouse model shows age-dependent susceptibility to brain injury, similar to the human condition, with strong lethality when mice are fed a high-lysine diet (HLD) at weaning.[12,13] KO mice that survive into adulthood have severe neuropathological alterations, with neuronal loss, vacuolation, and (in some cases) intraventricular hemorrhages.[14,15]

Studies using these KO mice have been key for developing novel therapeutic strategies. Notably, feeding the KO mice a low lysine, high glucose diet decreased the accumulation of neurotoxic metabolites in the brain,[16] which is why most patients currently receive this type of diet in combination with an oral supplement of L-carnitine. This strategy considerably decreases the frequency of acute encephalopathic episodes and, therefore, mortality.[17] However, despite the efforts made for early detection, by including this disease in the newborn screening programs and dietary treatment, some patients still develop encephalopathic crises.[9]

Here, we have explored the feasibility of gene therapy for GA1 based on the intravenous administration of an adeno-associated virus 9 (AAV9) that transports the *GCDH* gene. We demonstrate that a single intravenous injection of AAV-*GCDH* in neonatal *Gcdh* KO mice decreases GA and 3-OHGA accumulation, ameliorates striatal injury, and rescues the lethal phenotype of mice fed an HLD.

RESULTS

Intravascular delivery of AAV9-*GCDH* driven by the CAG promoter displays GCDH expression in brain and prevents C5DC accumulation

We constructed two AAV9 vectors expressing the human *GCDH* gene, one under the control of the phosphoglycerate kinase (PGK) promoter (AAV-P-GCDH), and one under the control of the chimeric cytomegalovirus (CMV) enhancer and chicken β-actin promoter (CAG) promoter (AAV-GCDH) (Figure 1A). The PGK promoter was chosen for its ability to drive mild expression of the transgenes, whereas the CAG promoter has been widely shown to exhibit strong expression of the controlled genes.[18,19] Since GCDH deficiency mostly leads to neuropathological alterations, we selected the AAV serotype AAV9 for its widespread transduction of the CNS parenchyma and its ability to cross the blood-brain barrier after intravascular delivery.[20,21] Tail vein injection of AAV-P-GCDH or AAV-GCDH at a dose of
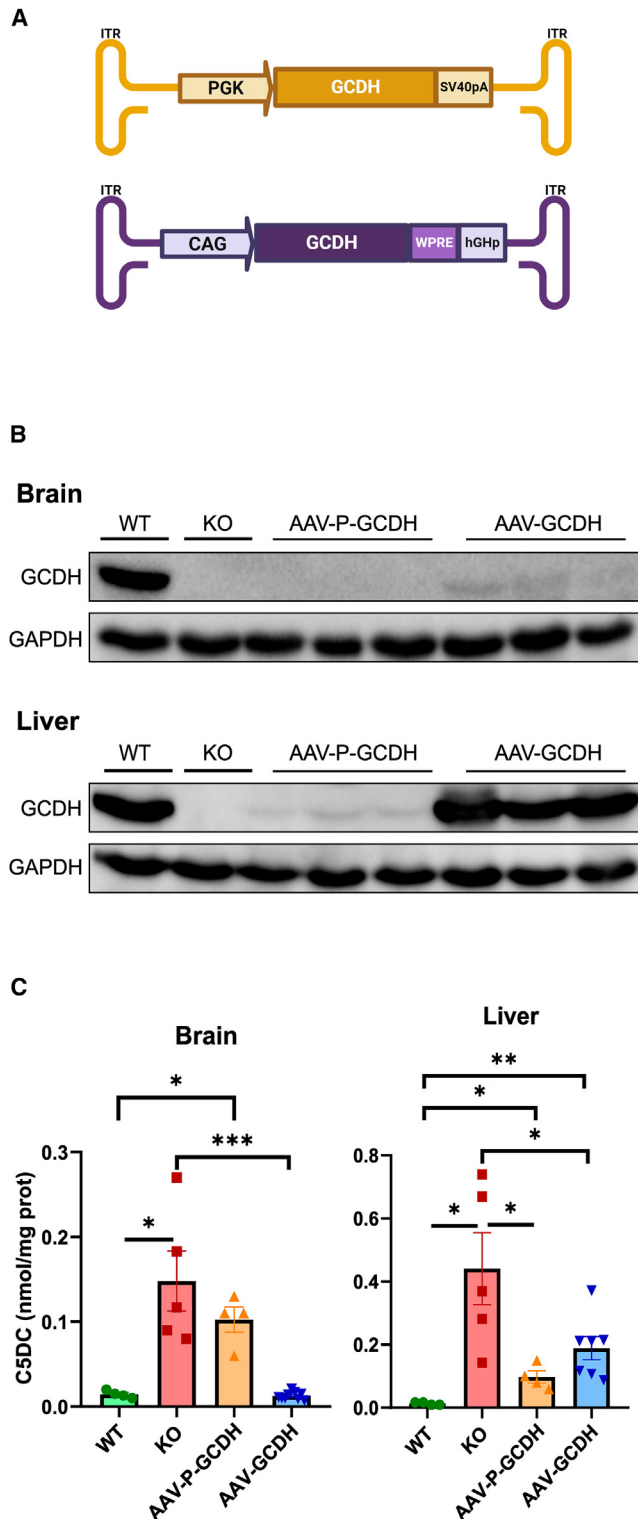
Figure 1. AAV9 vector expressing GCDH from the CAG promoter shows superior phenotype amelioration than that expressed from the PGK promoter

(A) Schematic illustration of the AAV-P-GCDH and AAV-GCDH vectors. (B) Western blot analysis of GCDH in liver and brain extracts from 6-week-old *Gcdh* KO mice treated with 7.5×10^{12} vg/kg of the indicated virus ($n = 3$). (C) C5DC content in liver and brain extracts from WT, KO, or KO-treated animals with AAV-P-GCDH or AAV-GCDH ($n = 4$ to 9). Data are expressed as the means ± SEM. Significance was assessed using a two-tailed Mann-Whitney test. $*p < 0.05$, $**p < 0.01$, $***p < 0.001$.
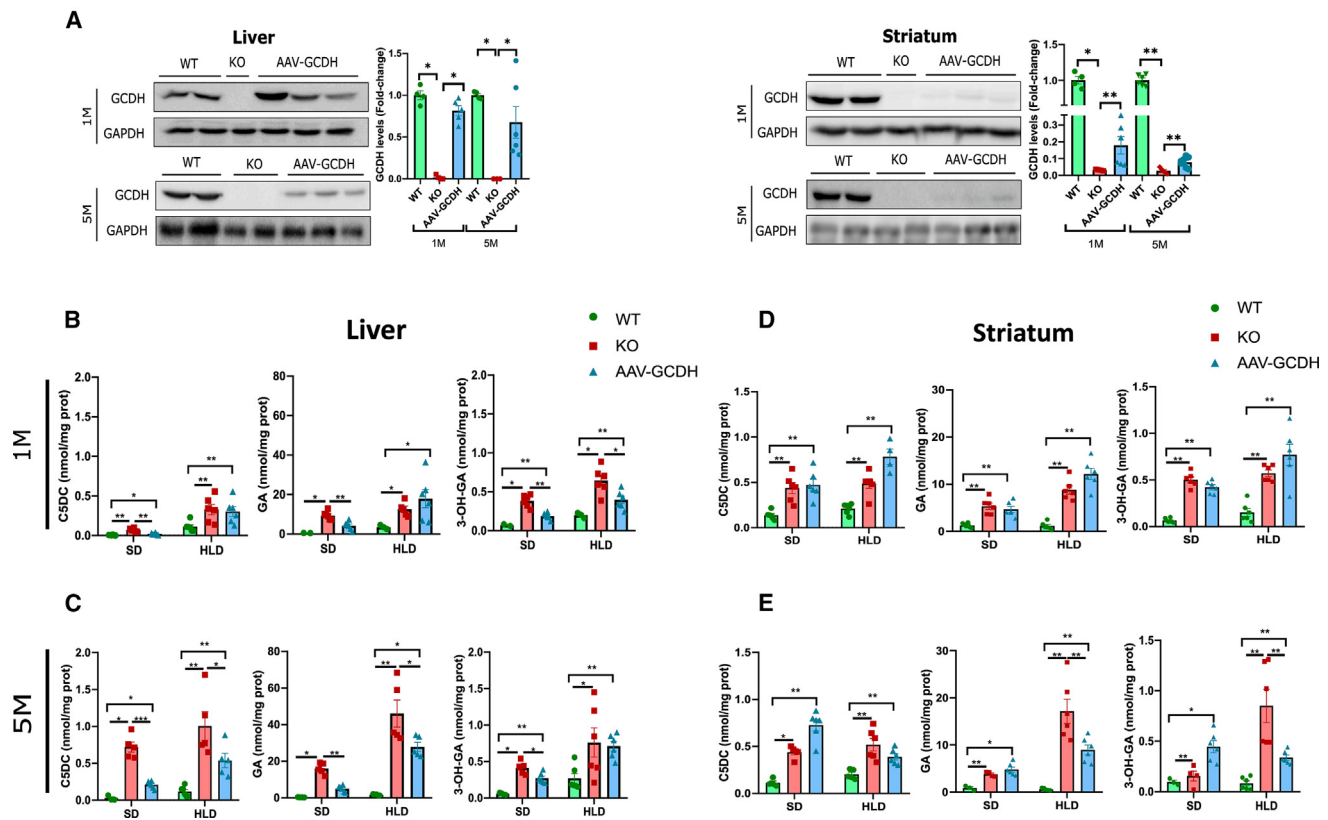
Figure 2. Intravascular administration of AAV-GCDH in KO young adult mice improves metabolite accumulation in the liver and in the striatum after HLD exposure at 5 months after treatment

AAV-GCDH was injected via tail vein at a dose (7.5×10^{12} vg/kg) into 1-month-old mice; 1 week later, mice were placed onto an HLD regime, or kept on a standard diet (SD), for 3 weeks or 5 months. (A) Western blot analysis of GCDH in liver and striatum lysates at 1 month and 5 months after treatment. Quantification of GCDH from different individuals ($n = 4$–6). C5DC, GA, and 3-OH GA were measured in WT, KO, and KO-AAV-GCDH treated mice in the liver at 1 month (B) or 5 months (C) after therapy, and in the striatum at 1 month (D) or 5 months (E) after therapy. Data are expressed as the means ± SEM. Significance was assessed using a two-tailed Mann-Whitney test. Statistical significance between WT-standard diet and WT-HLD were observed for C5DC in (B, D, and E) and for GA and 3-OH GA in (C). Statistical significance between KO-standard diet and KO-HLD were observed for GA in (C, D, E) and for 3-OH GA in (B, E). *$p < 0.05$, **$p < 0.01$, ***$p < 0.001$.

7.5×10^{12} vg/kg into 4-week-old *Gcdh* KO mice resulted in the recovery of GCDH expression in the liver with both vectors (albeit to much higher levels with AAV-GCDH). However, transgene expression in the brain was only observed in mice receiving the AAV-GCDH (Figure 1B). To assess the potential of the *GCDH* transgene to modulate the tissue accumulation of metabolites in KO mice, we measured the C5DC content. Notably, both AAV-P-GCDH and AAV-GCDH were able to decrease the accumulation of C5DC in the liver of treated *Gcdh* KO mice. However, only AAV-GCDH was able to decrease the content of this metabolite in the brain (Figure 1C). Thus, we chose the AAV construct with the CAG promoter as the candidate virus to evaluate the potential of GA1 gene therapy.

Intravenous AAV-GCDH delivery to young *Gcdh* KO mice prevents accumulation of diet-induced metabolites in target tissues up to 5 months after therapy

Next, we explored whether the AAV-GCDH vector could rescue the phenotype of the *Gcdh* KO mice, and especially their severe phenotype induced by feeding an HLD regime. KO mice were injected in the tail vein with a single dose of 7.5×10^{12} vg/kg AAV-GCDH at 4 weeks of age. One week later, treated or non-treated (control) animals were placed on a standard diet or an HLD for 1 month or 5 months. Mice were euthanized at 2 months of age (corresponding with 1 month after therapy) or 6 months of age (5 months after therapy), and tissues were analyzed for GCDH expression, enzyme activity, vector biodistribution, and metabolite accumulation. GCDH was expressed in the liver of treated KO mice at similar levels as in wild-type (WT) mice at 1 month after treatment, but the expression decreased after 5 months (Figure 2A). Expression of GCDH was analyzed in the striatum, as the targeted brain region of GA1 neuropathology. Low levels of GCDH were detected at both time points (Figure 2A). Consistently, GCDH activity was detected at both ages in the liver, but not in the striatum (Figure S1A). The analyses of C5DC, GA, and 3-OHGA revealed an increase in all the metabolite content in KO mice fed a standard diet, in line with previously reported studies.[11] A statistically significant decrease in all these metabolites was observed in the liver of
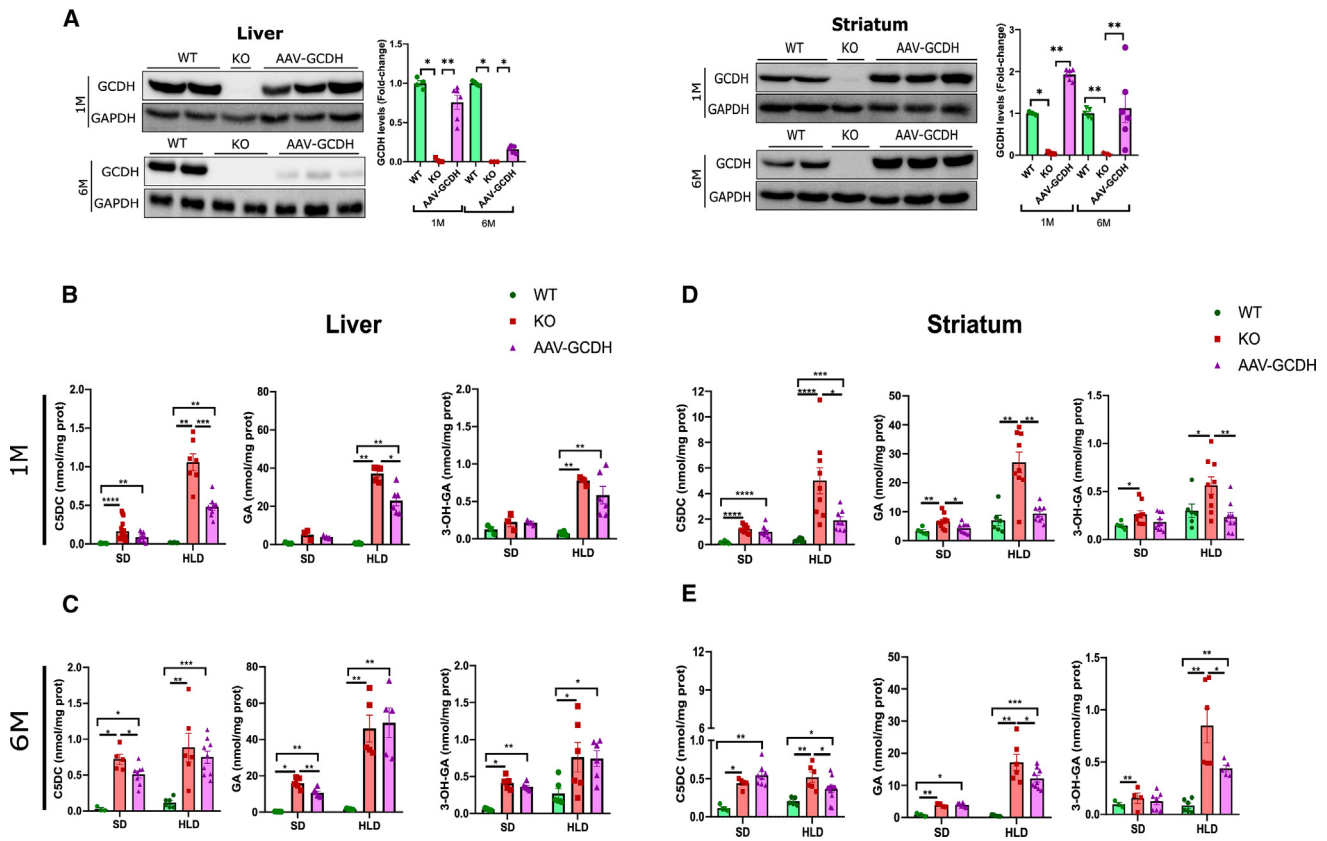
Figure 3. Intravascular administration of AAV-GCDH in KO-neonatal mice restores enzyme activity and prevents HLD-induced metabolite accumulation in the striatum at 1 month and 6 months after treatment

AAV-GCDH was injected into the temporal vein (at 5×10^{13} vg/kg) at P1, and at weaning were fed a standard diet (SD) or an HLD for 4 days or 5 months. Readouts were performed at 1 month and 6 months after viral injection. (A) Western blot analysis of GCDH in liver and striatum lysates at 1 month and 6 months after treatment. Quantification of GCDH from different individuals is shown (n = 4–6). C5DC, GA, and 3-OH GA concentrations in liver are shown for 1 month (B) and 6 months (C) after therapy, and in the striatum at 1 month (D) or 6 months (E) after therapy. Data are expressed as the means ± SEM. Significance was assessed using a two-tailed Mann-Whitney test. Statistical significance between WT-standard diet and WT-HLD were observed for C5DC in (E), and for GA and 3-OH GA in (C). Statistical significance between KO-standard diet and KO-HLD were observed for C5DC (B and D), GA (B–E), and 3-OHGA (B, D, E). *$p < 0.05$, **$p < 0.01$, ***$p < 0.001$.

treated KO mice fed a standard diet, and this reduction lasted until 5 months after therapy (Figures 2B and 2C). Placing mice on an HLD regime increased some of the metabolites, both in WT and KO mice, with the highest accumulation seem in the HLD-fed KO mice (herein, KO-HLD). The HLD increase in metabolite concentrations could be partially compensated by the therapy, with the 3-OHGA content significantly reduced with 1 month of therapy, and the C5DC and GA with 5 months of therapy (Figures 2B and 2C). Analysis of the metabolite content in the striatum showed that treatment with AAV-GCDH did not correct the levels of the C5DC, GA, or 3-OHGA metabolites when mice were fed a standard diet (Figures 2D and 2E). Similar to what we observed in the liver, HLD also triggered accumulation of some metabolites in WT and KO mice, again with the highest content in KO-HLD animals. However, a decrease in GA and 3-OHGA after 5 months of an HLD were observed in the striatum of treated mice (Figures 2D and 2E). These results suggest that increased sustained expression of GCDH for

5 months could be sufficient to prevent HLD-induced metabolite accumulation in target tissues.

Intravascular neonatal AAV-GCDH administration improves the phenotype of *Gcdh* KO mice exposed to an HLD

Since GA1 pathologic events impact individuals in early infancy, the effects of *GCDH* gene therapy would be particularly desirable at early stages of life to prevent the development of encephalopathic crises. We, therefore, considered evaluating the effects of AAV-GCDH therapy upon administration in neonatal mice.

Gcdh KO mice were injected with 5×10^{13} vg/kg of AAV-GCDH vector into the temporal vein at the neonatal P1 stage. At 25 days after injection, mice were placed onto a standard diet or an HLD regime for 4 days or for 5 months; mice were then euthanized at 1 or at 6 months after treatment. GCDH expression at 1 month after therapy showed high levels of the transgene in both liver and striatum (Figure 3A).
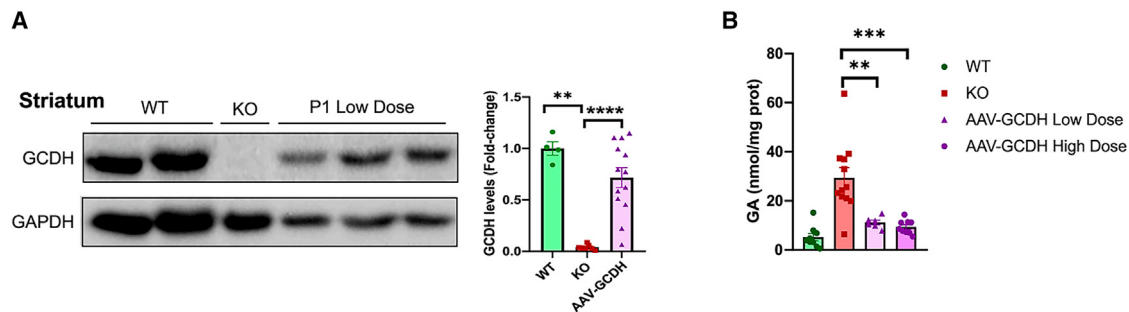
Figure 4. Intravascular administration of AAV-GCDH in KO-neonatal mice prevents from HLD-induced GA accumulation in the striatum at 1 month after therapy

AAV-GCDH were injected in the temporal vein at a dose 7.5×10^{12} vg/kg (Low dose) at P1. At weanling were exposed to HLD for 4 days. Analysis were performed 1 month after viral injection. (A) Western blot analysis of GCDH in the striatum. Quantification of GCDH from different individuals ($n = 6$). (B) Analysis of GA concentration ($n = 6$). Results also show the GA concentration of AAV-GCDH treated mice at 5×10^{13} vg/kg (Figure 3D; high dose). Data are expressed as the means ± SEM. Significance was assessed using a two-tailed Mann-Whitney test. $*p < 0.05$, $**p < 0.01$, $***p < 0.001$.

At 6 months after therapy, there was a decrease in the liver GCDH content (Figure 3A). Notably, although there was some decrease in GCDH expression in the striatum at 6 months after treatment as compared with 1 month after treatment, GCDH levels stayed similar to those of WT mice (Figure 3A). The differences in the persistence of GCDH expression between organs could be due to a dilution effect related to organ growth. In fact, the brain weight of C57BL/6J mice from postnatal day 17 (P17) to P60 does not show significant differences whereas there is more than a 4-fold increase in the mouse liver from P21 to P60.[22,23] Nevertheless, we cannot exclude the presence of other contributing factors, such as the rate of cellular turnover in the different organs. The persistence of GCDH activity was detected both at 1 and 6 months after therapy in the tissues analyzed (Figure S1B). Analysis of metabolites in the liver of treated mice showed metabolite correction at 1 month after therapy; however, this was not sustained at 6 months after treatment in KO-HLD mice, probably due to the reduced expression of GCDH in the liver at this age (Figures 3B and 3C). Interestingly, AAV-GCDH therapy corrected the accumulation of C5DC and the neurotoxic metabolites GA and 3-OHGA in the striatum of the KO-HLD mice, at both 1 and 6 months after therapy (Figures 3D and 3E). Correction of GA metabolites was also observed when applied a lower dose of 7.5×10^{12} vg/kg (Figure 4). Since GA1 pathology induced by the GA and 3-OHGA toxicity results in selective striatal degeneration we analyzed neuronal integrity by measuring N-acetyl aspartate (NAA) and its derivative metabolite, NAA glutamate (NAAG), by ^{1}H nuclear magnetic resonance spectroscopy (MRS) in the striatum. A statistically significant decrease in the NAA+NAAG content was observed in HLD *Gcdh* KO mice that was partially rescued by treatment (Figure 5A). Moreover, magnetic resonance imaging (MRI) analysis revealed extensive brain injury in KO-HLD mice, as shown by reduced mean diffusivity (MD), which was less evident in KO-HLD mice at 1 month after AAV-GCDH therapy (Figure 5B). Voxel-wise statistical analysis of the MD maps between WT and KO-HLD mice revealed extensive areas of significant differences, whereas WT and AAV-GCDH-treated KO-HLD mice showed greater similarities, again suggesting the rescue of the brain damage in treated mice (Figure S2).

Exposure of weanlings to an HLD has been associated with vacuolation, myelin pathology, and signs of gliosis.[13,24] Histopathology of striatum of *Gcdh* KO mice on an HLD confirmed irregular vacuolation with increased vacuole size after chronic feeding with HLD for 5 months. No changes were observed in WT mice on either a standard diet or an HLD (Figure S3). Interestingly, AAV-GCDH prevented large vacuole formation (Figure 6). Importantly, AAV-GCDH administration to *Gcdh* KO mice on a standard diet did not show virus-related histopathological findings, suggesting the safety of the treatment (Figure S3). Astrocyte damage analyzed by glial fibrillary acidic protein (GFAP) immunostaining, showed abundant GFAP in KO-HLD mice, in line with a diet-induced gliosis, but was almost absent after therapy (Figure 6). Myelin basic protein (MBP) staining revealed a progressive hypomyelination already present in older KO mice on a standard diet, with an enhanced decrease in the number of myelinated areas in the striatum of KO-HLD mice, after a 1- or 5-month diet regime. AAV-GCDH-treated mice were partially rescued for hypomyelination (Figure 6). However, immunohistochemistry against NeuN showed no differences in the neuronal count between the different groups, thus discarding significant neuronal loss (Figure S4).

Exposure to an HLD at this early stage of development has lethal consequences in the *Gcdh* KO mouse model.[13] Under our conditions, close to 50% of *Gcdh* KO mice died after 10 days on an HLD regime, and only 40% of KO mice survived 5 months on an HLD. Strikingly, however, all KO-HLD mice that received a neonatal AAV-GCDH treatment survived. Visual observation of treated KO-HLD mice in their cages show spontaneous locomotor activity similar to WT animals. Further, all KO-HLD-treated mice remained phenotypically normal, with no signs of disease progression, during the 150-day follow-up (Figure 7). These results suggest that neonatal AAV-GCDH gene therapy is effective in the diet-induced GA1 preclinical model.

DISCUSSION

GA1 is currently treated by dietary lysine restriction and carnitine supplementation. Unfortunately, almost one-third of affected
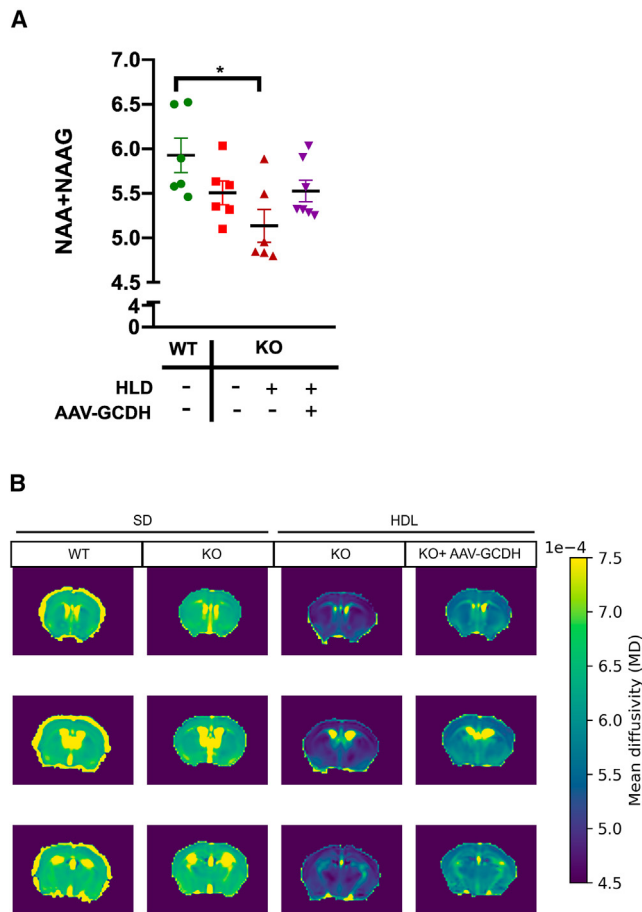
Figure 5. MRIs

One month-old WT or KO mice were fed a standard diet (SD) or HLD regime for 4 days and either treated with AAV-GCDH or saline; mice were then used for the MRI studies. (A) Proton MR spectroscopy imaging was performed in mice striatum ($n = 6$-7). Estimated concentration of NAA+NAAG are indicated. Data are expressed as the means ± SEM. Significance was assessed using a two-tailed Mann-Whitney test. *$p < 0.05$. (B) Representative brain images of MD maps obtained from DWI.

children do not respond to therapy and experience striatal degeneration despite neonatal screening and careful clinical management.[6–8] In the current study, we evaluated the potential of AAV-GCDH gene therapy in a preclinical mouse model of GA1. The application of the therapy faced the challenge to restore GCDH function in target organs and to protect the brain from injury, while using a minimally invasive approach. Our data show that a single systemic administration, through intravascular delivery of an AAV serotype 9 vector engineered to express the GCDH enzyme, ameliorated the striatal damage of *Gcdh* KO mice exposed to an HLD regime and rescued mice survival. These findings provide the foundation for translating AAV-GCDH gene therapy to GA1 patients.

We observed that the vector engineered with the CAG promoter was capable of inducing GCDH expression not only in the liver, but, importantly, also in key brain regions of the GA1 neuropathology.

When we used a virus with the weak promoter of PGK, we observed low GCDH expression in liver and no expression in brain after administration to young mice. This inefficiency was probably the result of the low promoter activity, together with the contribution of other distinct elements in the AAV expression cassettes, such as the polyadenylation signals SV40pA versus hGHpA and the presence of the Woodchuck hepatitis virus post-transcriptional regulatory element in the AAV-GCDH, a well-known element that stimulates transgene expression.[25] The low GCDH expression observed in brain even after AAV-GCDH administration was most probably related to the limited transduction of the CNS by AAV9 in young adults, as compared with the widespread effect in neonates.[21] In fact, even with the use of a strong CAG promoter, only low levels of expression were achieved in the striatum of young adult mice, whereas neonatal administration of the virus at an equivalent viral dose (of 7.5×10^{12} vg/kg) displayed superior GCDH levels in the striatum. At a higher dose (of 5×10^{13} vg/kg), the AAV-GCDH resulted in GCDH expression that was superior to that of WT animals. Interestingly, the virus with the PGK promoter showed some expression in brain when delivered neonatally at the highest dose, but at low levels (Figure S5). Even though high levels of striatal GCDH expression were achieved when the administered dose was 6.6-fold higher in neonatal mice as compared with young mice, the quantification of viral genomes at 1 month after AAV-GCDH delivery resulted in at least 40-fold more viral particles in the striatum after neonatal injection than after young mouse administration (Figure S6), showing that this delivery strategy has increased striatal transduction. Moreover, the fact that neonatal delivery of AAV9 vectors transduced both neuronal and glial cells favors neonatal delivery, since GA1 neurons and astrocytes display vulnerabilities to the accumulated metabolites.[21,26,27]

Neonatal AAV-GCDH administration prevented the accumulation of GA, 3-OHGA, and C5DC in the striatum of *Gcdh* KO-HLD mice after 1 month of treatment, as well as at 6 months after treatment after chronic HLD exposure. However, under a standard diet regime, few metabolites showed decreased content, suggesting that the AAV-GCDH therapy is insufficient to decrease the already accumulated metabolites, but is efficient in preventing their induction under HLD. Feeding the KO mice an HLD regime provoked biochemical and neuropathological alterations that highly resemble the encephalopathic crises that occur in individuals with GA1. Increased levels of GA and 3-OHGA are believed to trigger the striatal damage. In fact, it has been proposed that intracerebral *de novo* synthesis, and subsequent trapping of these metabolites, are the origin of their accumulation in the CNS of GA1 individuals.[28] Several authors have shown that there is limited flux of GA and 3-OHGA metabolites across the blood-brain barrier.[28,29] However, recent data have challenged this view; for instance, in a series of transplantation experiments, Barzi and collaborators[30] show that alterations in hepatic lysine catabolism affect the accumulation of toxic metabolites in the brain of *Gcdh* KO mice, and that restoring the liver GCDH in these mice via an AAV vector expressing GCDH from a liver-specific promoter partially rescued the phenotype. However, very high doses (of approximately 15 times higher than the ones used here) were needed to observe such benefits.[30]
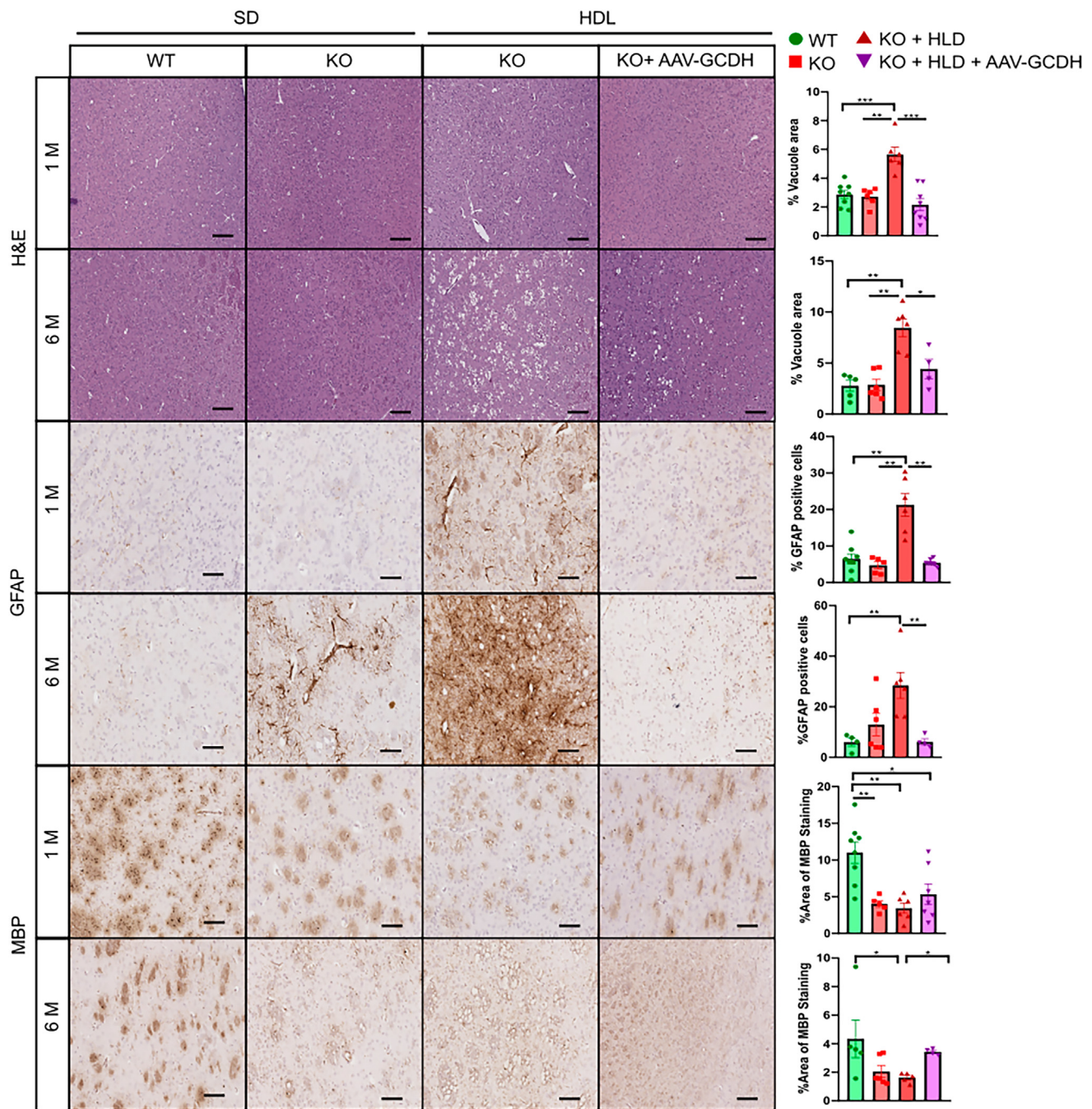
Figure 6. Neonatal AAV-GCDH ameliorates striatal injury

Immunohistochemical analysis of striatum alterations in the indicated groups of mice. Hematoxylin and eosin staining showing progressive vacuolation in KO-HLD mice. Scale bar, 50 μm, and GFAP, glial marker; scale bar, 100 μm, and MBP, myelin marker. Quantification was performed on histology images with 1 section/mouse, digitalized with a ScanScope slide scanner, and analyzed with QuPath 0.3.0 software. Results are presented as percentage of vacuole area, GFAP-positive cells, or area of MBP staining. Data are expressed ase the means ± SEM. Significance was assessed using a two-tailed Mann-Whitney test. *$p < 0.05$, **$p < 0.01$, ***$p > 0.001$.

We also observed some contribution of liver correction when AAV-GCDH was administered to young adult (4-week-old) mice, and sustained GCDH expression was achieved for at least 5 months, improving the metabolite content both in the liver and in circulation (Figure S7). However, this was not observed when the therapy was given in the neonatal period, probably because the dilution effect
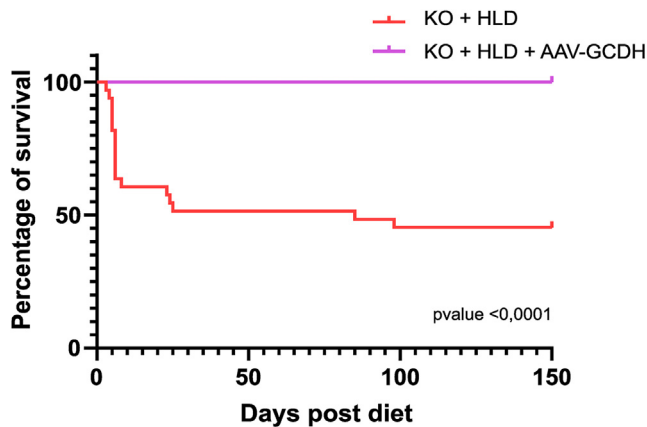
Figure 7. Neonatal AAV-GCDH administration to KO-HLD mice results in normal lifespan

Follow-up of 150 days for mice survival in *Gcdh* KO mice treated (n = 25) or not (n = 33) with AAV-GCDH and exposed to HLD at weaning. *p* value was calculaed by log rank test (Mantle-Cox).

related to organ growth hindered a full recovery of the GCDH expression and the metabolite reduction after 6 months of treatment. Thus, it could be speculated that, below a certain threshold of liver GCDH activity, local GCDH delivery is required to prevent an increase of metabolites in the striatum and to protect the brain from damage, as our data show after neonatal delivery. This is in line with the reported benefits of delivering GCDH to the central nervous system.[31]

The mechanisms by which GA and 3-OHGA generate brain damage are not fully understood. Some studies emphasize disturbances in the glutamatergic and GABAergic neurotransmission, facilitating excitotoxic mechanisms.[14,15] Moreover, oxidative stress and mitochondrial dysfunction also contribute to the pathology.[32] The main alterations associated with striatal injury in GA1 individuals are reactive astrogliosis, neuronal loss, and changes in white matter.[33,34] Our results show that *Gcdh* KO mice exposed to an HLD had a significantly lower content of NAA+NAAG metabolites in the striatum, which can be partially rescued by prior AAV-GCDH therapy. Decreased levels of NAA have also been observed in GA1 individuals[35,36] and have been associated with neuronal loss or neuronal distress. However, the absence of significant differences in the NeuN staining between all the experimental settings in this study discards neuronal death in the striatum. Previous reports have also shown absence of neuronal loss in the *Gcdh* KO mice, which could be attributed to low neuronal vulnerability of these mice to neurotoxic metabolites.[11,24] However, decreases in NAA levels may reflect impaired mitochondrial function, suggesting neuronal dysfunction.[37] Nevertheless, we observed severe striatal damage with a strong astrogliosis in the *Gcdh* KO animals that progressed with age and with HLD feeding, which could however be rescued by the therapy.

An increased glial immunoreactivity when exposed to an HLD has been associated with increased GA and 3-OHGA concentrations, causing oxidative stress.[26] In line with previous reports, our data

also showed strong vacuolation inside the axonal packages with decreased myelinated areas.[11,13,24] We also observed a progression of the lesions after chronic exposure to HLD, with major alterations after 5 months of HLD. Notably, a remarkable improvement in the neuropathology was observed at 1 month after therapy. Partial rescue was also observed in mice that developed a highly severe phenotype induced by 5 months of HLD exposure. Alterations in myelination have been proposed to alter synaptogenesis, and the rescue of hypomyelination reverses synaptic deficits.[38] Thus, we could speculate that protecting from demyelination with the AAV-GCDH treatment would lead to a recovery of neuronal function. In fact, our MRI findings confirmed the rescue of the neuronal damage and white matter alterations. These results support the view that neonatal delivery of AAV-GCDH provide neuroprotection to HLD-induced striatal injury in *Gcdh* KO mice, and that the amelioration of the phenotype leads to the survival of all treated KO mice.

Our data highlight the considerable therapeutic potential AAV-GCDH gene therapy for the treatment of individuals with GA1. We propose a noninvasive vector delivery approach with high efficacy that, when administered to pediatric patients, could potentially protect them from developing acute encephalopathic crises.

MATERIALS AND METHODS

Plasmid design and AAV vector generation

To generate the pAAV-CAG-GCDH, the GCDH cDNA (Harvard Institute of Proteomics, HsCD00002837) was cloned into the pAAV-CA (Plasmid # 69616, Addgene), under the control of the ubiquitous CAG promoter (chimeric promoter with the CMV enhancer and the CAG). To generate the pAAV-PGK-GCDH, the human PGK promoter (kindly provided by JC: Segovia), the SV40 polyA (pCMVβ, Clontech) and the GCDH cDNA were cloned in the NOT I site of the pAAV-MCS (Agilent Technologies). AAV vectors were produced according to standard procedures at the Viral Vector Production Unit, Autonomous University of Barcelona.

Western blot analysis

Total protein extracts were obtained using lysis buffer (10 mM Tris-HCl [pH 6.8], 4% SDS, and 20% glycerol) containing 1% Complete Mini Protease Inhibitor (Roche). Lysates were boiled for 10 min at 98°C and centrifuged 5 min at 16,000×g. Protein concentration was determined by BCA Protein Assay kit (Thermo Fisher Scientific). Protein samples were resolved in 10% SDS-PAGE and transferred to PVDF membranes by standard methods. Membranes were blocked with TBS-Tween 10% milk (1 h at room temperature), immunoblotted with the corresponding antibody (anti-GCDH, AV43559, Sigma-Aldrich; or anti-GAPDH, ABS16, Sigma-Aldrich) diluted in TBS-Tween 1% milk, rinsed with TBS-Tween, and incubated with a polyclonal goat anti-rabbit horseradish peroxidase-conjugated antibody (1/2,000 in TBS-Tween 1% milk, 1 h at room temperature). Antibody labeling was detected using the ECL Amersham Prime Western Blotting Detection Reagent (GE Healthcare Life Sciences).

GCDH in gel activity

GCDH activity was analyzed by blue native polyacrylamide gel electrophoresis using an adaptation of the originally described methodology.[39] Briefly, liver and striatum from WT and GCDH KO mice were Dounce homogenized (20 strokes) in lysis buffer (225 mM mannitol, 75 mM sucrose, 10 mM Tris-HCl, and 0.1 mM EDTA) on ice. Tissue homogenates were centrifuged twice at $650 \times g$ for 20 min at 4°C to remove cell debris and nuclei. Protein concentrations were determined using a BCA assay. Mitochondria-enriched fractions were obtained from 1,500 μg of liver protein, or from 1,000 μg of striatum protein, by centrifugation ($10,000 \times g$ 10 min at 4°C). Samples were solubilized in 50 mM Bis-Tris, 0.5 M EDTA, 750 mM aminocaproic acid in the presence of 2% N-dodecyl-beta-maltoside, loaded onto 4%–20% polyacrylamide gradient gels, and electrophoresed in nondenaturing conditions. GCDH activity was detected by incubating the gel in an activity buffer (50 mM phosphate buffer, 200 μM glutaryl-CoA, 1.5 μM FAD, and 2 mg/mL NBT) at 37°C overnight.

Biochemical analysis

Cell extracts were obtained as described above. C5DC were extracted from cell extracts or serum samples with an organic solvent containing deuterated C5DC used as internal standard (NeoBase 1 kit, PerkinElmer). The extracted product was dried under nitrogen and reconstituted in methanol/H_2O (75/25). For neuronal tissue, the dried extracted product was derivatized with n-butanol/HCl 3N, dried under nitrogen and reconstituted in methanol/H_2O (75/25). The analysis was then performed with direct infusion using the mobile phase and chromatographic conditions as manufacture description in Neobase 1 kit and in positive MRM mode using an ultra performance liquid chromatography-tandem mass spectrometry (I-Class ACQUITY UPLC system; XevoTQD). Results were quantified using Neolynx Software (Waters).

For GA and 3-OHGA analysis, an aqueous solution containing the deuterium-labeled internal standards GA-d4 and 3-OH-GA-d5 was added to the homogenized striatum samples. Compounds were extracted using an Oasis HLB 96-well plate (60 mg sorbent) and eluted using an acetonitrile/methanol (90/10) phase, after formic acid at 0.4% solution was added to facilitate ionization. Chromatographic separation was done with an ACQUITY Premier BEH C18 Column (1.7 μm, 2.1 × 100 mm) and analyzed in negative MRM mode by H-Class ACQUITY UPLC system-XevoTQS. The flow rate was set to 320 μL min^{-1} using a binary mixture of solvent A (water with 0.1% formic acid) and solvent B (methanol with 0.1% formic acid). Values were quantified with Targetlynx Software (Walters) using a calibration curve and normalized for protein content.

Animal procedures

$Gcdh^{-/-}$ KO mice were purchased from the Mutant Mouse Resource and Research Center strain ID 34368 and maintained in an specific pathogen-free animal facility in a 12-h dark-light cycle. Mice were fed ad libitum with a standard diet or a HL containing 4.7% Lys, as stated. Animals were placed on an HLD as 3-week-old weanlings or 5-week-old young adults. Mice were sacrificed at the age of 1, 2, or 6 months.

$Gcdh$ KO mice were injected in the temporal vein (neonatal) or tail vein (4-week-old young adults) with 1×10^{11} or 1.5×10^{10} viral genomes of AAV9-GCDH or AAV9-PGK-GCDH. Based on weight, neonatal mice received a single dose of 5×10^{13} vg/kg or 7.5×10^{12} vg/kg, and young adults received 7.5×10^{12} vg/kg. Neonatal injections were performed following the previously described protocol.[40] Briefly, pups at P1 or P2 were place on wet ice for 30–60 s to anesthetize them and then placed under a stereoscope. The temporal vein was identified, the needle containing the virus was inserted into the vein, and the viral content was released. Pups were then coated with bedding to ensure acceptance by the mothers and placed back into the home cage.

Animal procedures met the guidelines of European Community Directive 86/609/EEC and the local legislation (Decret 214/1997 of 20 July by the Department d'Agricultura, Ramaderia i Pesca de la Generalitat de Catalunya) under the approval of the Experimental Animal and Ethical Committee of the University of Barcelona.

Histological preparation and immunohistochemical analysis

Mice were transcardially perfused with 1% PBS followed by 4% paraformaldehyde. Brains were removed and postfixed in 4% paraformaldehyde for 24 h at 4°C and embedded in paraffin. Serial 6 μm brain coronal sections were collected on glass slides. Sections were processed for antigen retrieval in citrate buffer (Citrate Buffer 10× pH 6.0 1, Sigma-Aldrich) at 100°C (boiling point) for 5 min in a pressure cooker.

Sections were treated with a blocking solution (PBS 1×, 10% FBS, 1% BSA, 0.3% Triton X-100) for 1.5 h at room temperature and incubated overnight at 4°C with primary antibodies (anti-GFAP, G3893, Sigma-Aldrich; Anti-NeuN, clone A60, Sigma-Aldrich and anti-MBP, clone SMI 94, Biolegend) diluted in PBS with 0.1% BSA. Endogenous peroxidase was blocked with Dual Endogenous Enzyme Block (Dako) for 10 min at room temperature. The reaction was developed using Dako EnVision + Dual Link System-HRP (DAB+) (Dako), and tissues were counterstained with Harris hematoxylin (Panreac). Stained sections were visualized with an Olympus BX51 vertical microscope and digitalized with a ScanScope slide scanner and analyzed with QuPath 0.3.0 software.

MRI studies

MRI experiments were performed in a cohort of 24 mice (12 female and 12 male) distributed into 4 experimental groups: WT on a standard diet, $n = 6$; KO on a standard diet and no treatment, $n = 6$; KO on an HLD but no treatment, $n = 6$; and KO on an HLD and with treatment, $n = 6$.

MRI acquisitions were performed on a 7.0T BioSpec 70/30 horizontal animal scanner (Bruker BioSpin), equipped with an actively shielded gradient system (400 mT/m, 12-cm inner diameter). The

receiver coil was a one-channel phased-array surface coil for the mouse brain. The acquisition protocol included MRS and diffusion-weighted imaging (DWI). Three-dimensional localizer scans were used to ensure the accurate position of the head at the isocenter of the magnet. MRS in a voxel placed located in striatum was acquired using PRESS (voxel size 5.4 µL, repetition time [TR] = 5,000 ms, echo time [TE] = 12 ms, 256 averages and partial water suppression using VAPOR). Voxel position was based on reference T2-weighted images in axial, sagittal and coronal orientation acquired with a RARE sequence (voxel size = $0.08 \times 0.08 \times 0.16$ mm^3, TR = 2,300 ms, TE = 11 ms, RARE factor = 8). A non-suppressed reference water signal was also acquired in the same voxel as reference for absolute metabolite quantification. DWI were acquired with a two-shell scheme including 6 gradient directions acquired with b-value = 500 s/mm^2 and 30 gradient directions with b = 1,000 s/mm^2 and 4 baseline images acquired without diffusion weighting. Other parameters were TR = 4,000 ms, TE = 27.7 ms, and voxel size = $0.21 \times 0.21 \times 0.5$ mm^3.

Metabolite concentration was estimated using LC-Model.[41] To ensure quality of the estimations, spectrum was only included if full-width at half-maximum was lower than 0.08 ppm and signal-to-noise ratio was greater than 10. Metabolites quantified with relative Cramér-Rao lower bounds of higher than 20% were discarded.

DWI were processed to extract MD maps using dipy.[42] Processing includes eddy current correction, denoising and unbias, registration to T2 to correct for EPI distortion and fitting of diffusion tensor (DT) model. Fractional Anisotropy (FA) and MD at each voxel were obtained from the estimated DT. Voxel-based statistical analysis was performed using FMRIB Software Library (FSL) randomize using threshold-free cluster enhancement (TFCE) and family-wise error to correct for multiple comparisons.[43]

Viral genome quantification
Genomic DNA was purified from frozen tissue using standard procedures. Viral genomes were analyzed by Real Time qPCR, on a QuantStudio7 System (Applied Biosystems), using SYBR Green I Master plus mix (Roche Diagnostics) and the primer set specific for the AAV2 ITR genome sequences (Fwd ITR primer, 5′-GG AACCCCTAGTGATGGAGTT and Rev ITR primer, 5′-CGGC CTCAGTGAGCGA).[44] Viral genomes were quantified by interpolation in a standard curve of pAAV-GCDH DNA dilutions in a background of genomic DNA.

Statistical analysis
Experimental data are represented by the mean ± SEM of at least three independent experiments. Statistical analysis was performed on GraphPad Prism v8.0.1 (GraphPad Software). Statistical differences were evaluated using a 2-tailed non-parametric Mann-Whitney test. A p value of <0.05 was taken as the level of significance. Mice survival was analyzed by the Kaplan-Meier method and evaluated with a log-rank (Mantel-Cox) test.

DATA AND CODE AVAILABILITY
Data are available within the published article and supplemental files. Additional data are available from corresponding author on reasonable request.

SUPPLEMENTAL INFORMATION
Supplemental information can be found online at https://doi.org/10.1016/j.omtm.2024.101276.

AUTHOR CONTRIBUTIONS
A.M.-B. designed and performed most of the experiments and prepared the figures; E.S.-B. and J.G.-V. performed the metabolite analysis; S.G.-S. contributed to the AAV design and generation; E.M.-M. performed MRI acquisition and analysis; E.S.-B. and F.T. performed GCDH enzyme activity assays; A.R. provided GA1 pathology expertise and contributed to manuscript writing; M.J.B. and M.A. helped with immunostainings and interpretation of CNS pathology; C.F. coordinated the study and wrote the manuscript.

DECLARATION OF INTERESTS
The authors declare no competing interests.

REFERENCES
1. Goodman, S.I., and Kohlhoff, J.G. (1975). Glutaric aciduria: inherited deficiency of glutaryl-CoA dehydrogenase activity. Biochem. Med. *13*, 138–140. https://doi.org/10.1016/0006-2944(75)90149-0.

2. Boy, N., Mühlhausen, C., Maier, E.M., Ballhausen, D., Baumgartner, M.R., Beblo, S., Burgard, P., Chapman, K.A., Dobbelaere, D., Heringer-Seifert, J., et al. (2023). Recommendations for diagnosing and managing individuals with glutaric aciduria type 1: Third revision. J. Inherit. Metab. Dis. *46*, 482–519. https://doi.org/10.1002/jimd.12566.

3. Schuurmans, I.M.E., Dimitrov, B., Schröter, J., Ribes, A., de la Fuente, R.P., Zamora, B., van Karnebeek, C.D.M., Kölker, S., and Garanto, A. (2023). Exploring

genotype-phenotype correlations in glutaric aciduria type 1. J. Inherit. Metab. Dis. *46*, 371–390. https://doi.org/10.1002/jimd.12608.

4. Busquets, C., Merinero, B., Christensen, E., Gelpí, J.L., Campistol, J., Pineda, M., Fernández-Alvarez, E., Prats, J.M., Sans, A., Arteaga, R., et al. (2000). Glutaryl-CoA dehydrogenase deficiency in Spain: evidence of two groups of patients, genetically, and biochemically distinct. Pediatr. Res. *48*, 315–322. https://doi.org/10.1203/00006450-200009000-00009.

5. Garbade, S.F., Greenberg, C.R., Demirkol, M., Gökçay, G., Ribes, A., Campistol, J., Burlina, A.B., Burgard, P., and Kölker, S. (2014). Unravelling the complex MRI pattern in glutaric aciduria type I using statistical models-a cohort study in 180 patients. J. Inherit. Metab. Dis. *37*, 763–773. https://doi.org/10.1007/s10545-014-9676-9.

6. Kyllerman, M., Skjeldal, O., Christensen, E., Hagberg, G., Holme, E., Lönnquist, T., Skov, L., Rotwelt, T., and von Döbeln, U. (2004). Long-term follow-up, neurological outcome and survival rate in 28 Nordic patients with glutaric aciduria type 1. Eur. J. Paediatr. Neurol. *8*, 121–129. https://doi.org/10.1016/j.ejpn.2003.12.007.

7. Kölker, S., Garbade, S.F., Greenberg, C.R., Leonard, J.V., Saudubray, J.-M., Ribes, A., Kalkanoglu, H.S., Lund, A.M., Merinero, B., Wajner, M., et al. (2006). Natural history, outcome, and treatment efficacy in children and adults with glutaryl-CoA dehydrogenase deficiency. Pediatr. Res. *59*, 840–847. https://doi.org/10.1203/01.pdr.0000219387.79887.86.

8. Strauss, K.A., Williams, K.B., Carson, V.J., Poskitt, L., Bowser, L.E., Young, M., Robinson, D.L., Hendrickson, C., Beiler, K., Taylor, C.M., et al. (2020). Glutaric acidemia type 1: Treatment and outcome of 168 patients over three decades. Mol. Genet. Metabol. *131*, 325–340. https://doi.org/10.1016/j.ymgme.2020.09.007.

9. Boy, N., Mengler, K., Heringer-Seifert, J., Hoffmann, G.F., Garbade, S.F., and Kölker, S. (2021). Impact of newborn screening and quality of therapy on the neurological outcome in glutaric aciduria type 1: a meta-analysis. Genet. Med. *23*, 13–21. https://doi.org/10.1038/s41436-020-00971-4.

10. Kölker, S., Boy, S.P.N., Heringer, J., Müller, E., Maier, E.M., Ensenauer, R., Mühlhausen, C., Schlune, A., Greenberg, C.R., Koeller, D.M., et al. (2012). Complementary dietary treatment using lysine-free, arginine-fortified amino acid supplements in glutaric aciduria type I - A decade of experience. Mol. Genet. Metabol. *107*, 72–80. https://doi.org/10.1016/j.ymgme.2012.03.021.

11. Koeller, D.M., Woontner, M., Crnic, L.S., Kleinschmidt-DeMasters, B., Stephens, J., Hunt, E.L., and Goodman, S.I. (2002). Biochemical, pathologic and behavioral analysis of a mouse model of glutaric acidemia type I. Hum. Mol. Genet. *11*, 347–357. https://doi.org/10.1093/hmg/11.4.347.

12. Zinnanti, W.J., Lazovic, J., Housman, C., LaNoue, K., O'Callaghan, J.P., Simpson, I., Woontner, M., Goodman, S.I., Connor, J.R., Jacobs, R.E., and Cheng, K.C. (2007). Mechanism of age-dependent susceptibility and novel treatment strategy in glutaric acidemia type I. J. Clin. Invest. *117*, 3258–3270. https://doi.org/10.1172/JCI31617.

13. Zinnanti, W.J., Lazovic, J., Wolpert, E.B., Antonetti, D.A., Smith, M.B., Connor, J.R., Woontner, M., Goodman, S.I., and Cheng, K.C. (2006). A diet-induced mouse model for glutaric aciduria type I. Brain *129*, 899–910. https://doi.org/10.1093/brain/awl009.

14. Rodrigues, M.D.N., Seminotti, B., Amaral, A.U., Leipnitz, G., Goodman, S.I., Woontner, M., de Souza, D.O.G., and Wajner, M. (2015). Experimental evidence that overexpression of NR2B glutamate receptor subunit is associated with brain vacuolation in adult glutaryl-CoA dehydrogenase deficient mice: A potential role for glutamatergic-induced excitotoxicity in GA I neuropathology. J. Neurol. Sci. *359*, 133–140. https://doi.org/10.1016/j.jns.2015.10.043.

15. Busanello, E.N.B., Fernandes, C.G., Martell, R.V., Lobato, V.G.A., Goodman, S., Woontner, M., de Souza, D.O.G., and Wajner, M. (2014). Disturbance of the glutamatergic system by glutaric acid in striatum and cerebral cortex of glutaryl-CoA dehydrogenase-deficient knockout mice: possible implications for the neuropathology of glutaric acidemia type I. J. Neurol. Sci. *346*, 260–267. https://doi.org/10.1016/j.jns.2014.09.003.

16. Sauer, S.W., Opp, S., Hoffmann, G.F., Koeller, D.M., Okun, J.G., and Kölker, S. (2011). Therapeutic modulation of cerebral L-lysine metabolism in a mouse model for glutaric aciduria type I. Brain *134*, 157–170. https://doi.org/10.1093/brain/awq269.

17. Kölker, S., Christensen, E., Leonard, J.V., Greenberg, C.R., Burlina, A.B., Burlina, A.P., Dixon, M., Duran, M., Goodman, S.I., Koeller, D.M., et al. (2007). Guideline for the diagnosis and management of glutaryl-CoA dehydrogenase deficiency (gluta-

ric aciduria type I). J. Inherit. Metab. Dis. *30*, 5–22. https://doi.org/10.1007/s10545-006-0451-4.

18. Xu, L., Daly, T., Gao, C., Flotte, T.R., Song, S., Byrne, B.J., Sands, M.S., and Parker Ponder, K. (2001). CMV-beta-actin promoter directs higher expression from an adeno-associated viral vector in the liver than the cytomegalovirus or elongation factor 1 alpha promoter and results in therapeutic levels of human factor X in mice. Hum. Gene Ther. *12*, 563–573. https://doi.org/10.1089/104303401300042500.

19. Haurigot, V., Marcó, S., Ribera, A., Garcia, M., Ruzo, A., Villacampa, P., Ayuso, E., Añor, S., Andaluz, A., Pineda, M., et al. (2013). Whole body correction of mucopolysaccharidosis IIIA by intracerebrospinal fluid gene therapy. J. Clin. Invest. *123*, 3254–3271. https://doi.org/10.1172/JCI66778.

20. Zincarelli, C., Soltys, S., Rengo, G., and Rabinowitz, J.E. (2008). Analysis of AAV serotypes 1-9 mediated gene expression and tropism in mice after systemic injection. Mol. Ther. *16*, 1073–1080. https://doi.org/10.1038/mt.2008.76.

21. Foust, K.D., Nurre, E., Montgomery, C.L., Hernandez, A., Chan, C.M., and Kaspar, B.K. (2009). Intravascular AAV9 preferentially targets neonatal neurons and adult astrocytes. Nat. Biotechnol. *27*, 59–65. https://doi.org/10.1038/NBT.1515.

22. Zong, W., Liu, S., Wang, X., Zhang, J., Zhang, T., Liu, Z., Wang, D., Zhang, A., Zhu, M., and Gao, J. (2015). Trio gene is required for mouse learning ability. Brain Res. *1608*, 82–90. https://doi.org/10.1016/j.brainres.2015.02.040.

23. Gong, T., Zhang, C., Ni, X., Li, X., Li, J., Liu, M., Zhan, D., Xia, X., Song, L., Zhou, Q., et al. (2020). A time-resolved multi-omic atlas of the developing mouse liver. Genome Res. *30*, 263–275. https://doi.org/10.1101/GR.253328.119.

24. Olivera-Bravo, S., Seminotti, B., Isasi, E., Ribeiro, C.A., Leipnitz, G., Woontner, M., Goodman, S.I., Souza, D., Barbeito, L., and Wajner, M. (2019). Long Lasting High Lysine Diet Aggravates White Matter Injury in Glutaryl-CoA Dehydrogenase Deficient (Gcdh-/-) Mice. Mol. Neurobiol. *56*, 648–657. https://doi.org/10.1007/s12035-018-1077-x.

25. Loeb, J.E., Cordier, W.S., Harris, M.E., Weitzman, M.D., and Hope, T.J. (1999). Enhanced expression of transgenes from adeno-associated virus vectors with the woodchuck hepatitis virus posttranscriptional regulatory element: implications for gene therapy. Hum. Gene Ther. *10*, 2295–2305. https://doi.org/10.1089/10430349950016942.

26. Olivera-Bravo, S., Ribeiro, C.A.J., Isasi, E., Trías, E., Leipnitz, G., Díaz-Amarilla, P., Woontner, M., Beck, C., Goodman, S.I., Souza, D., et al. (2015). Striatal neuronal death mediated by astrocytes from the Gcdh-/- mouse model of glutaric acidemia type I. Hum. Mol. Genet. *24*, 4504–4515. https://doi.org/10.1093/hmg/ddv175.

27. Mateu-Bosch, A., Segur-Bailach, E., García-Villoria, J., Gea-Sorlí, S., Ruiz, I., del Rey, J., Camps, J., Guitart-Mampel, M., Garrabou, G., Tort, F., et al. (2024). Modeling Glutaric Aciduria Type I in human neuroblastoma cells recapitulates neuronal damage that can be rescued by gene replacement. Gene Ther. *31*, 12–18. https://doi.org/10.1038/S41434-023-00428-8.

28. Sauer, S.W., Okun, J.G., Fricker, G., Mahringer, A., Müller, I., Crnic, L.R., Mühlhausen, C., Hoffmann, G.F., Hörster, F., Goodman, S.I., et al. (2006). Intracerebral accumulation of glutaric and 3-hydroxyglutaric acids secondary to limited flux across the blood-brain barrier constitute a biochemical risk factor for neurodegeneration in glutaryl-CoA dehydrogenase deficiency. J. Neurochem. *97*, 899–910. https://doi.org/10.1111/j.1471-4159.2006.03813.x.

29. Keyser, B., Glatzel, M., Stellmer, F., Kortmann, B., Lukacs, Z., Kölker, S., Sauer, S.W., Muschol, N., Herdering, W., Thiem, J., et al. (2008). Transport and distribution of 3-hydroxyglutaric acid before and during induced encephalopathic crises in a mouse model of glutaric aciduria type 1. Biochim. Biophys. Acta *1782*, 385–390. https://doi.org/10.1016/j.bbadis.2008.02.008.

30. Barzi, M., Johnson, C.G., Chen, T., Rodriguiz, R.M., Hemmingsen, M., Gonzalez, T.J., Rosales, A., Beasley, J., Peck, C.K., Ma, Y., et al. (2023). Rescue of glutaric aciduria type I in mice by liver-directed therapies. Sci. Transl. Med. *15*, eadf4086. https://doi.org/10.1126/scitranslmed.adf4086.

31. Guo, L., Li, Z., Li, Y., Qu, B., Jiao, G., Liang, C., Lu, Z., Wang, X.-G., Huang, C., Du, H., et al. (2022). Treatment of glutaric aciduria type I (GA-I) via intracerebroventricular delivery of GCDH. Fundamental Research *2*, 836–842. https://doi.org/10.1016/j.fmre.2022.08.013.

32. Wajner, M., Amaral, A.U., Leipnitz, G., and Seminotti, B. (2019). Pathogenesis of brain damage in glutaric acidemia type I: Lessons from the genetic mice model. Int. J. Dev. Neurosci. *78*, 215–221. https://doi.org/10.1016/j.ijdevneu.2019.05.005.

33. Funk, C.B.R., Prasad, A.N., Frosk, P., Sauer, S., Kölker, S., Greenberg, C.R., and Del Bigio, M.R. (2005). Neuropathological, biochemical and molecular findings in a glutaric acidemia type 1 cohort. Brain *128*, 711–722. https://doi.org/10.1093/brain/awh401.

34. Soffer, D., Amir, N., Elpeleg, O.N., Gomori, J.M., Shalev, R.S., and Gottschalk-Sabag, S. (1992). Striatal degeneration and spongy myelinopathy in glutaric acidemia. J. Neurol. Sci. *107*, 199–204. https://doi.org/10.1016/0022-510x(92)90289-w.

35. Kurul, S., Cakmakçi, H., and Dirik, E. (2004). Glutaric aciduria type 1: proton magnetic resonance spectroscopy findings. Pediatr. Neurol. *31*, 228–231. https://doi.org/10.1016/j.pediatrneurol.2004.02.009.

36. Pérez-Dueñas, B., De La Osa, A., Capdevila, A., Navarro-Sastre, A., Leist, A., Ribes, A., García-Cazorla, A., Serrano, M., Pineda, M., and Campistol, J. (2009). Brain injury in glutaric aciduria type I: the value of functional techniques in magnetic resonance imaging. Eur. J. Paediatr. Neurol. *13*, 534–540. https://doi.org/10.1016/j.ejpn.2008.12.002.

37. Barker, P.B. (2001). N-Acetyl Aspartate—A Neuronal Marker? Ann. Neurol. *49*, 423–424. https://doi.org/10.1002/ANA.90.

38. Wang, F., Yang, Y.-J., Yang, N., Chen, X.-J., Huang, N.-X., Zhang, J., Wu, Y., Liu, Z., Gao, X., Li, T., et al. (2018). Enhancing Oligodendrocyte Myelination Rescues Synaptic Loss and Improves Functional Recovery after Chronic Hypoxia. Neuron *99*, 689–701.e5. https://doi.org/10.1016/j.neuron.2018.07.017.

39. Wittig, I., Braun, H.-P., and Schägger, H. (2006). Blue native PAGE. Nat. Protoc. *1*, 418–428. https://doi.org/10.1038/nprot.2006.62.

40. Gombash Lampe, S.E., Kaspar, B.K., and Foust, K.D. (2014). Intravenous injections in neonatal mice. J. Vis. Exp. e52037. https://doi.org/10.3791/52037.

41. Provencher, S.W. (1993). Estimation of metabolite concentrations from localized in vivo proton NMR spectra. Magn. Reson. Med. *30*, 672–679. https://doi.org/10.1002/mrm.1910300604.

42. Garyfallidis, E., Brett, M., Amirbekian, B., Rokem, A., van der Walt, S., Descoteaux, M., and Nimmo-Smith, I.; Dipy Contributors (2014). Dipy, a library for the analysis of diffusion MRI data. Front. Neuroinf. *8*, 8. https://doi.org/10.3389/fninf.2014.00008.

43. Winkler, A.M., Ridgway, G.R., Webster, M.A., Smith, S.M., and Nichols, T.E. (2014). Permutation inference for the general linear model. Neuroimage *92*, 381–397. https://doi.org/10.1016/j.neuroimage.2014.01.060.

44. Aurnhammer, C., Haase, M., Muether, N., Hausl, M., Rauschhuber, C., Huber, I., Nitschko, H., Busch, U., Sing, A., Ehrhardt, A., and Baiker, A. (2012). Universal real-time PCR for the detection and quantification of adeno-associated virus serotype 2-derived inverted terminal repeat sequences. Hum. Gene Ther. Methods *23*, 18–28. https://doi.org/10.1089/hgtb.2011.034.